International Journal of Pharmaceutics 475 (2014) 613–623

Contents lists available at ScienceDirect

International Journal of Pharmaceutics

journal homepage: www.elsevier.com/locate/ijpharm

Development and characterization of co-loaded curcumin/triazole-halloysite systems and evaluation of their potential anticancer activity

Serena Riela [a,*], Marina Massaro [a], Carmelo G. Colletti [a], Alessandra Bommarito [b], Carla Giordano [b], Stefana Milioto [c], Renato Noto [a], Paola Poma [d], Giuseppe Lazzara [c,**]

[a] Dipartimento STEBICEF, sez. Chimica, Università degli Studi di Palermo, Viale delle Scienze, Parco d'Orleans II, Ed. 17, 90128 Palermo, Italy
[b] Dipartimento Biomedico di Medicina Interna e Specialistica, sez. Endocrinologia, Diabetologia, Metabolismo, Università degli Studi di Palermo, 90127 Palermo, Italy
[c] Dipartimento di Fisica e Chimica, Università degli Studi di Palermo, Viale delle Scienze, Parco d'Orleans II, Ed. 17, 90128 Palermo, Italy
[d] Dipartimento di Scienze per la Promozione della Salute e Materno Infantile "G. D'Alessandro", Area Funzionale di Farmacologia, Università di Palermo, Via del Vespro 129, 90127 Palermo, Italy

ARTICLE INFO

Article history:
Received 24 July 2014
Received in revised form 8 September 2014
Accepted 11 September 2014
Available online 16 September 2014

Keywords:
Halloysite nanotubes
Triazolium salts
Drug carrier
Curcumin
In vitro anticancer activity

ABSTRACT

Positively charged halloysite nanotubes functionalized with triazolium salts (f-HNT) were employed as a carrier for curcumin molecules delivery. The synthesis of these f-HNT new materials is described. Their interaction with curcumin was evaluated by means dynamic light scattering (DLS) and UV–vis spectroscopy in comparison with pristine unmodified HNT (p-HNT). The curcumin load into HNT was estimated by thermogravimetric analysis (TGA) measurements, while the morphology was investigated by scanning electron microscopy (SEM) techniques. Release of curcumin from f-HNT, at three different pH values, by means of UV–vis spectroscopy was also studied. Furthermore, different cancer cell lines were used to evaluate the potential cytotoxic effect of HNT at different concentrations and culture times. The results indicated that the f-HNT drug carrier system improves the solubility of curcumin in water, and that the drug-loaded f-HNT exerted cytotoxic effects against different cell lines.

1. Introduction

Phenolic compounds originated from one of the main class of secondary metabolites in plants, are natural phytochemicals mostly deriving from phenylalanine, which are widely present in food and nutraceuticals (Aggarwal et al., 2008). Among them, curcumin and its derivatives have been extensively studied and evaluated for their biological activity.

Curcumin [bis(4-hydroxy-3-methoxy-phenyl)-1,6-heptadiene-3,5-dione] is a natural phenolic compound isolated as a yellow pigment from the dried rhizome of *Curcuma longa*, a plant that is widely cultivated in tropical areas of Asia and Central America, commonly used as a spice, as a food colorant, and even as a food preservative. Several studies, also, report that it is an agent possessing a wide variety of biological and pharmacological activities, including anti-proliferation (Choi et al., 2006), anti-apoptosis (Aggarwal et al., 2008), anti-angiogenesis (Lin et al., 2007) and inhibition of cell invasion and metastasis (Chen et al., 2008).

Successful application of this compound is hampered, however, by the occurrence of some disadvantageous properties. Being hydrophobic in nature, curcumin is sparingly soluble in water (ca. 0.6 μg/mL). Moreover, it degrades rapidly under neutral or alkaline conditions, with a half-life shorter than 10 min in phosphate buffer solution at pH 7.2 (Kurien et al., 2007). As a result, its bioavailability is poor, particularly after oral or topical administration (Anand et al., 2007). Therefore, a carefully designed carrier could significantly facilitate curcumin delivery and broaden the range of its possible pharmaceutical applications.

Nanoscale drug delivery systems are an innovative approach for overcoming the aforementioned problems. Previous attempts at encapsulating curcumin in liposomes, phospholipid complexes, or other nanoparticle-based technologies have been reported, showing an improvement in water dispersibility and a longer circulation time (Tang et al., 2010; Duan et al., 2010; Kim et al., 2011)

A possible nanosized delivery system is constituted by naturally available clay halloysite nanotubes (HNT). Halloysite has been found a viable and inexpensive nanoscale container for the encapsulation of biologically active molecules such as biocides and drugs, as Price et al. (2001) first demonstrated.

* Corresponding author. Tel.: +39 9123897546; fax: +39 091596825.
** Corresponding author. Tel.: +39 9123897962.
E-mail addresses: serena.riela@unipa.it (S. Riela), giuseppe.lazzara@unipa.it (G. Lazzara).

http://dx.doi.org/10.1016/j.ijpharm.2014.09.019
0378-5173/

Halloysite is a hydrated polymorph of kaolinite consisting of silica on the outer surface and alumina at the innermost surface of the tubular structure (Bates et al., 1950). Therefore, the different inner and outer-compositions of these materials allow to accomplish different chemical reactions on either surface (Massaro et al., 2014a,b; Li et al., 2008; Du et al., 2010; Wang et al., 2008; Vergaro et al., 2010; Lvov et al., 2002; Matsuno et al., 2003, 2006; Ma et al., 2011, 2012; Terayama et al., 2010; Horiuchi et al., 2009).

The functionalization of HNT with organic salts is a good strategy to prepare a new class of materials presenting most of the features and properties of organic salt, allowing them to be dispersed in physiological media.

For the cellular internalization of nanoparticles in general, surface charge is, also, important in determining whether the nanoparticles would cluster in blood flow or would adhere to, or interact with oppositely charged cells membrane (Feng, 2004). A cationic surface is desirable as it promotes the interaction between the nanoparticles and the cells, and hence increases the rate and extent of internalization (Shenoy and Amiji, 2005).

In the last years triazolium derivatives have attracted the attention of scientists because the *N*-alkyl-1,2,3-triazoles moiety is easily accessible through the versatile copper-catalyzed (CuAAC) [2 + 3] cycloaddition (Huisgen, 1963; Meldal and Tornoe 2008; Finn and Fokin, 2010).

Triazoles and their derivatives, indeed, occupy a central position (Noël et al., 2009) amongst the most significant compounds that constitute pharmaceutically and medicinally important drug centers (Al-Masoudi et al., 2006). Several triazoles have been reported to possess antibacterial (Singh et al., 2006), antifungal (Rezaei et al., 2009), antitumor (Guo-Qiang et al., 2008), plant growth regulating (Jin et al., 2007) and cytotoxic (Bagihalli et al., 2008) activities.

In this work we report the selective functionalization of halloysite nanotubes at the external surface with triazolium salts and the interaction of these nanomaterials with curcumin. The functionalization served for two purposes: (i) introducing a positive charge on the halloysite carrier; (ii) verifying whether the presence of the biological active triazolium moiety could exert a synergic effect with curcumin.

2. Experimental

2.1. Materials and methods

All reagents and materials needed were used as purchased (Aldrich), without further purification.

Halloysite was supplied by Applied Minerals. This material has an average tube diameter of 50 nm and inner lumen diameter of 15 nm. Typical specific surface area of this halloysite is 65 m^2/g; pore volume of ~1.25 mL/g; refractive index 1.54; and specific gravity 2.53 g/cm^3.

The 3-azidopropyltrimethoxysilane was synthetized as previously reported (Karl and Buder, 1983).

UV–vis spectra were recorded on a Beckmann DU 650 spectrometer.

IR spectra were recorded with an Agilent Technologies Cary 630 FTIR spectrometer. Specimens for measurements were prepared by mixing 5 mg of the sample powder with 100 mg of KBr.

An ESEM FEI QUANTA 200 F microscope was used to study the morphology of the functionalized HNTs. Before each experiment, the sample was coated with gold under argon by means of an Edwards Sputter Coater S150A to avoid charging under the electron beam.

Thermogravimetric analyses were performed on a Q5000 IR apparatus (TA Instruments) under a nitrogen flow (25 $cm^3\,min^{-1}$ for the sample and 10 $cm^3\,min^{-1}$ for the balance). The weight of each sample was ca. 10 mg. The measurements were carried out by heating the sample from room temperature up to 900 °C at a rate of 10 °C min^{-1}. The difference between the thermoanalytical curve of loaded HNT or f-HNT and the corresponding pristine nanoparticles was calculated, in order to highlight the degradation of the curcumin present in the composites.

The DLS measurements were performed at 22.0 ± 0.1 °C in a sealed cylindrical scattering cell at a scattering angle of 90°, by means of a Brookhaven Instrument apparatus composed of an BI-9000ATcorrelator and a He–Ne laser (75 mW) at a wavelength (λ) of 632.8 nm. The solvent was filtered by means of a Millipore filter with 0.45 μm pore size. For all systems, the field-time

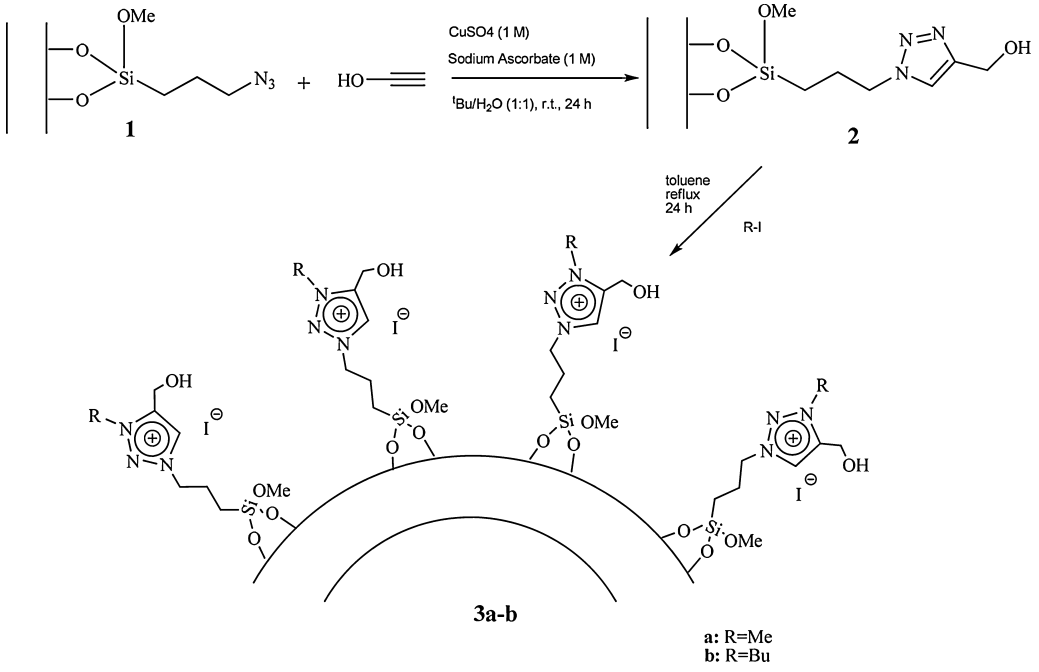

Scheme 1. Synthesis of functionalized f-HNT**3a-b**.

autocorrelation functions were well described by a mono-exponential decay function, which provides the decay rate (Γ) of the single diffusive mode. For the translational motion, the collective diffusion coefficient at a given concentration is $D_t = \Gamma/q^2$ where q is the scattering vector given by $4\pi n\lambda^{-1}\sin(\theta/2)$ where n is the water refractive index and θ is the scattering angle.

Turbidimetric measurements were performed with a Beckmann DU 650 spectrometer.

ζ-potential measurements were performed by means of a ZETASIZER NANO ZS90 (Malvern Instruments).

The dispersions were sonicated with an ultrasound bath VWR Ultrasonic Cleaner (power 200 W, frequency 75 MHz).

2.2. Syntheses

2.2.1. Synthesis of compound **1**

In a typical synthetic run, 100 mL of 3-azidopropyl trimethoxysilane was dissolved in 20 mL of dry toluene and 1 g of clay powder was added. The suspension was first dispersed under ultrasonic irradiation for 15 min, and then refluxed for 16 h under stirring. Afterwards, the crude solid filtered off, washed with several aliquots of MeOH and dried overnight at 80 °C under vacuum.

Whitish powder: 0.95 g.

IR (KBr): ν = 2103 (*s*, ν_s N_3).

TGA: loss peak of 1.5% at a temperature of 254 °C.

2.2.2. General synthesis of compound **2**

Compound **1** (500 mg) was suspended in a H_2O/*t*-BuOH 1:1 mixture (4 mL) *t* and propargyl alcohol (20.7 mg, 10 eq) was added. The mixture was stirred under argon in the presence of catalytic amount of $CuSO_4$/sodium ascorbate solution (1 M, 1:10 v/v) at room temperature for 24 h. After this time, the solvent was filtered off, the powder was rinsed with H_2O, then with MeOH and finally dried at 80 °C under vacuum.

IR(KBr): ν = 2937 (*w*), 2885(*w*, *s*, ν_s CH_2); 1641(*s*, ν_s C═N), 1400 (*w*, ν_s N═N), 1324 (*w*, ν_s C—N).

TGA: weight loss of 2.3% in a range between 222 and 380 °C.

2.2.3. General procedure for the synthesis of compounds ***3a-b***

Compound **2** (100 mg) was suspended in dry toluene (10 mL) and an excess of the proper iodoalkane was added. The suspension was then refluxed at 120 °C for 24 h. After this time, the solid was filtered off, rinsed with CH_2Cl_2 and finally dried at 80 °C under vacuum.

3a: TGA: weight loss of 5.9% at temperature of 344 °C.

IR (KBr): ν = 2951 (*w*, ν C═C), 2927 (m), 2857(*w*, ν_s CH_2), 1630 (*s*, ν_s C═N), 1460 (w, ν_s N═N), 1320 (s, ν_s C—N).

3b: TGA: weight loss of 8.5% at temperature of 475 °C.

IR (KBr): ν = 2961 (*w*, ν C═C), 2949 (m), 2876 (*w*, ν_s CH_2), 1626 (*s*, ν_s C═N), 1462 (*w*, ν_s N═N), 1320 (*s*, ν_s C—N).

2.3. General procedure to obtain HNT/curcumin dispersions

Varying weighed amounts of p-HNT (from 1.2 up to 18 mg) or f-HNT**3a-b** (from 0.1 up to 0.9 mg) were dispersed by sonication for 5 min in the proper solvent, at an ultrasound power of 200 W and a temperature of 25 °C. 1 mL of curcumin solution in the solvent was added to the HNT dispersions. The final volume was 10 mL and 2 mL for p-HNT and f-HNT**3a-b** dispersions, respectively. Final curcumin concentration was 1×10^{-4} M.

2.4. Loading procedure

2.4.1. p-HNT

In order to encapsulate the curcumin inside the halloysite nanotubes, we mixed 20 mg of halloysite, as dry powder, with few milliliters of saturated solution of curcumin in ethanol. The suspension was sonicated for 5 min, at an ultrasound power of 200 W and a temperature of 25 °C and then was evacuated for

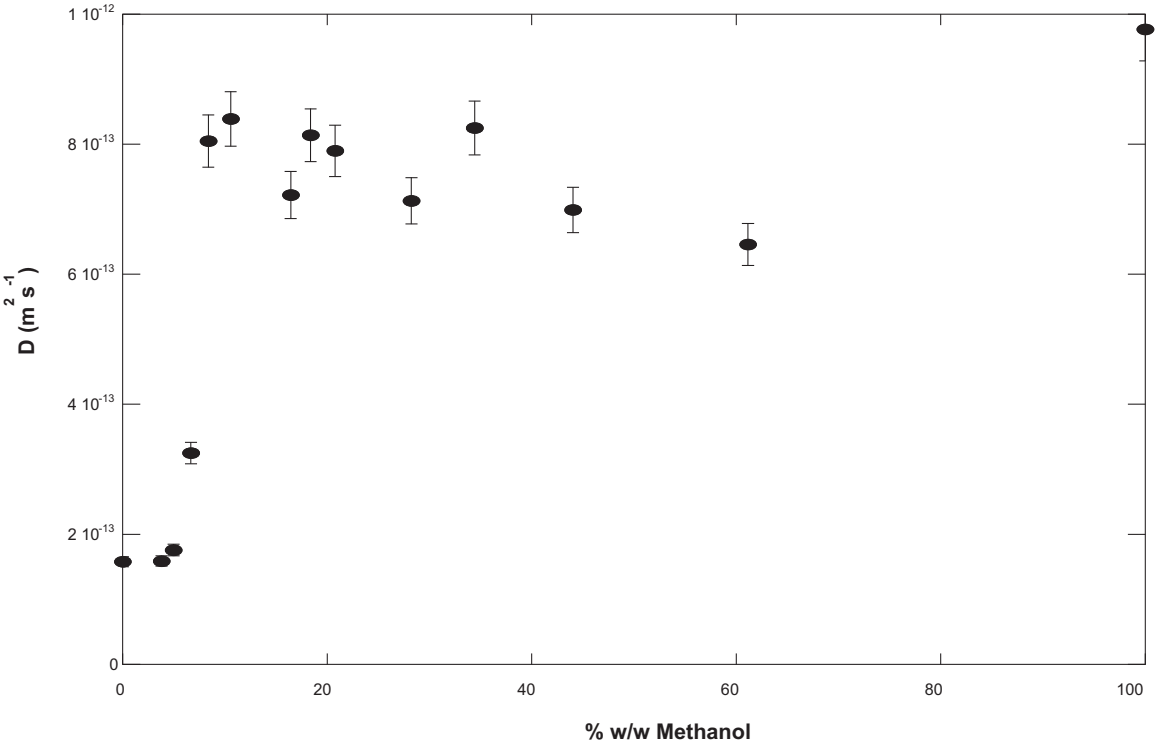

Fig. 1. Diffusion coefficient obtained by DLS measurements for **3b** as a function of different percent of methanol in methanol/water mixed media.

3 cycles. The powder was washed with H_2O and then dried at 80 °C under vacuum.

*2.4.2. f-HNT**3a-b***

To a dispersion of f-HNT**3a-b** in a water/methanol 9:1 (250 mL) mixture 2.5 mL of a curcumin solution 10^{-2} M in methanol were added. The obtained dispersion was stirred for 48 h at r.t. and then filtered off, washed with small amounts of water and finally dried at 60 °C under vacuum overnight.

2.5. Release kinetics

The release kinetics at 37 °C were evaluated in HCl 0.1 N, in phthalate buffer solution pH 5 or in phosphate buffer pH 8. UV–vis measurements were carried out by suspending 5 mg of HNT/Curc in 3 mL of the chosen solvent buffer. In all cases sink conditions were maintained.

2.6. Efficiency of curcumin loaded-halloysite and f-HNT3a.

The human papillary thyroid carcinoma cell line BCPAP and the human anaplastic thyroid carcinoma cell lines SW1736, 8505 C and C643 were kindly provided by Prof. F Frasca, University of Catania, Italy. BCPAP and 8505c were cultured in RPMI 1640 (PAA), supplemented with 10% FBS, 5% penicillin–streptomycin, and 5% glutamine. SW1736 and C643 cell line was cultured in DMEM (PAA), supplemented with 10% FBS, 5% penicillin–streptomycin, and 5% glutamine cultures were maintained in 5% CO_2 at 37 °C in a humidified incubator.

HA22T/VGH, HepG2 and Hep3B is a poorly differentiated hepatoma cell line which contains HBV integrants. It was cultured in Roswell Park Memorial Institute (RPMI) 1640 (HyClone Europe Ltd., Cramlington UK) supplemented with 10% heat-inactivated fetal calf serum, 2 mM L-glutamine, 1 mM sodium pyruvate, 100 units/ml penicillin and 100 mg/ml streptomycin (all reagents were from HyClone Europe) in a humidified atmosphere at 37 °C in 5% CO_2. Cells having a narrow range of passage number were used for all experiments.

2.7. Cell growth assays

2.7.1. MTS assay

In order to test the effects of the agents, the cells were seeded at 2×10^4 cells/well onto 96-well plates and then incubated overnight. At time 0, the medium was replaced with fresh complete medium and thereof curcumin, HNT/Curc or f-HNT **3a**/Curc, were added according to the concentrations indicated later. At the end of treatment, 16 μL of a commercial solution (Promega Corporation, Madison, WI, USA) containing 3-(4,5-dimethylthiazol-2-yl)-5-(3-carboxy methoxyphenyl)-2-(4-sulphophenyl)-2H-tetrazolium (MTS) and phenazine ethosulfate were added. The plates were incubated for 2 h in a humidified atmosphere at 37 °C under 5% CO_2. The bioreduction of the MTS dye was assessed by measuring the absorbance of each well at 490 nm. Cytotoxicity was expressed as a percentage of the absorbance measured in the control cells.

2.7.2. MTT assay

Cell proliferation was assessed by colorimetric assay using 3-(4,5-Dimethylthiazol-2-yl)-2,5-diphenyltetrazolium bromide (MTT). Cells were plated in 96-well plate at a density of 5×10^3cells/well and cultured up to 24, 48 and 72 h in the presence of HNT/Curc or f-HNT 3a/Curc. At the end of the incubation period the cells were incubated for 4 h at 37 °C with MTT; then the medium was removed and the cells were treated with DMSO for 5 min. Absorbance was read at 550 nm in a Multiskan FC microplate reader (Thermo Fisher Scientific).

Protocol to determine the amount of curcumin embedded into cells.

The amount of drug embedded into cells (C_{cell}) was determined by the following equation:

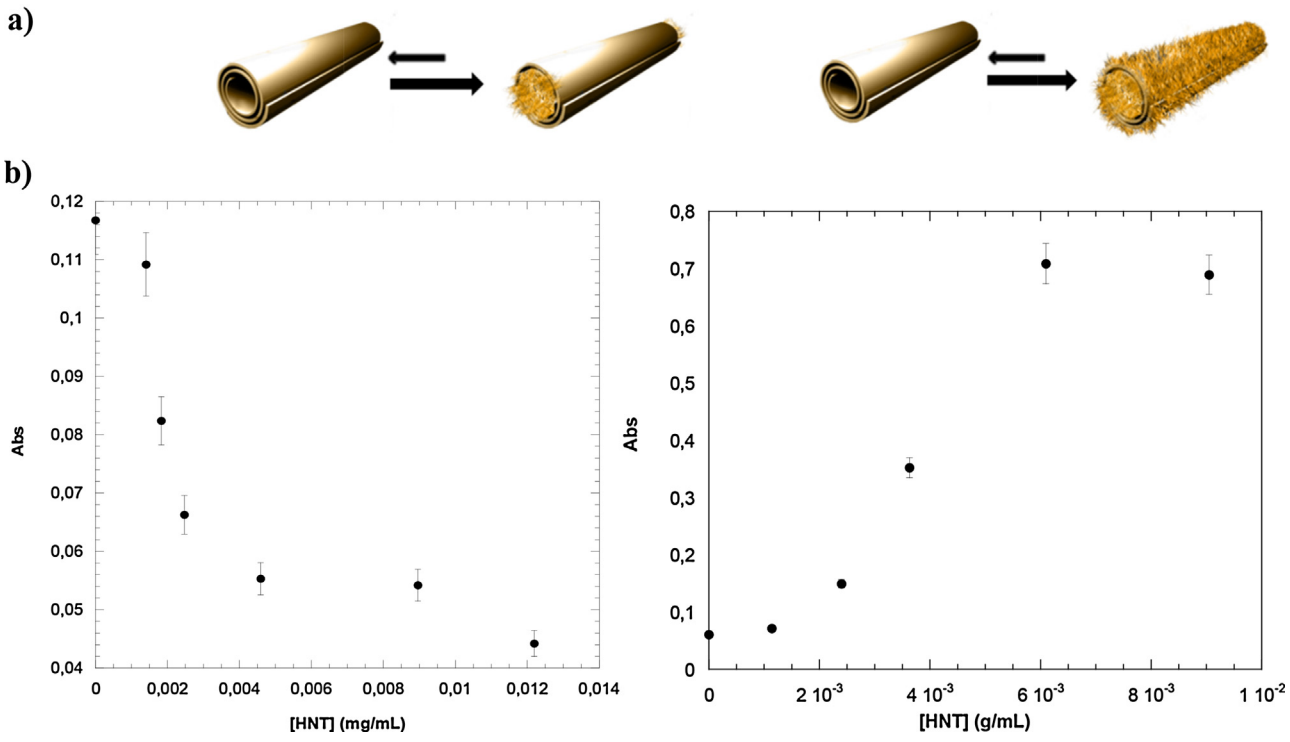

Fig. 2. Trend of the absorbance of the curcumin (1×10^{-4} M) as function of p-HNT concentration (from 0 to 1.8×10^{-3} g/mL) in (a) buffer solution, pH 8/MeOH 9:1 (λ_{max} = 360 nm); (b) H_2O/MeOH 9:1 (λ_{max} = 425 nm). The inset shows a representation cartoon of hypothesized equilibria.

$$C_{cell} = C_i - C_f \quad (1) \qquad (1)$$

where C_i is the concentration of curcumin associated to halloysite and C_f is the drug concentration in supernatant after incubation, respectively. The curcumin content in the supernatant was determined spectrophotometrically at 445 nm referring to a standard calibration curve.

3. Results and discussion

3.1. Synthesis and properties of functionalized halloysite nanotubes

The HNT-bearing random triazolium salts, f-HNT**3a-b**, were prepared according to the synthetic route shown in Scheme 1.

Starting with halloysite nanotubes treated with an excess of 3-azido-propyl trimethoxysilane, the compound **1** was prepared. After work-up the azido groups loading, estimated by TGA, was as large as 1.5%. The introduction of the triazole moiety, on the external surface of **1** by the CuAAC reaction, gave compound **2**, which was purified by repeated washing with water and methanol. Finally, compounds **3a-b** were prepared by dispersing **2** in toluene under ultrasound irradation, followed by addition of proper alkyl iodide.

FTIR investigation on **1**, **2**, **3** shows that the vibrational bands of HNT remain unchanged after the reactions (data are reported in SI). The frequency and assignments of each vibrational mode are based on previous halloysite reports (Yuan et al., 2008; Tonle et al., 2003; Vansant et al., 1995; White and Tripp, 2000; Madejova and Komadel, 2001; Vranken et al., 1992). Compared to p-HNT, **1** exhibits the CH_2 asymmetric and symmetric stretching at 2930 cm^{-1} and 2850 cm^{-1} respectively, the CH_2 scissoring at 1470 cm^{-1} and the stretching of the azido groups at 2103 cm^{-1}. In the **2** and **3a-b** compounds, the stretching of the aromatic H—C═, C═N, N═N, C—N groups around 3000, 1600, 1400 and 1320 cm^{-1} respectively are also observed. These findings evidence the presence of the silane moieties in **1** and triazolic groups in **2** and **3** and, based on the unaltered frequency of stretching bands of the OH of the inner-surface Al-OH groups, led to conclude that grafting has taken place only on the external surface of HNT.

The samples **3a-b** were investigated by means of TGA to determine the grafted amount of organic moieties (Fig. S.6 in SI). Three steps of mass loss were observed for **3a-b**. By comparison with the thermoanalytical curve for p-HNT, which presents two dehydration steps at ca. 500 and 700 °C, the **3a-b** show also a mass loss in the range from 200 to 400 °C accounting for the degradation and volatilization of the organic fractions. The grafting degree was determined by comparing the residual masses at 900 °C of each f-HNT and p-HNT; results as large as 6.1 wt% and 8.6 wt% were obtained for **3a** and **3b** respectively. The difference in the grafting degree is, of course, due to the different molecular weight of the grafted organic moieties.

Direct observation of the surface morphology of **3a** and **3b** was accomplished by SEM (see SI). In both cases the tubular shape of the nanoclay is not lost after grafting. Moreover, the lumen of the functionalized nanotubes appears empty, in agreement with the expected grafting at the external surface. The characteristic average size of the functionalized nanotubes are coincident with those observed for the p-HNT (Cavallaro et al., 2011).

3.2. Colloidal stability of f-HNT.

Turbidimetric analyses were performed to highlight the influence of functionalization on the dispersion stability of f-HNT in aqueous media, which might be crucial for possible application as drug carrier.

A dispersion of f-HNT**3a** showed a higher stability in water than **3b**, according to the more hydrophobic surface functionalization in **3b** as compared to **3a** (data are shown in Fig. S.9 of SI). These data can be interpreted under the light of the diffusion coefficient of the nanoparticles in the solvent. With the aim of using these new systems as drug carriers, we studied the stability of dispersions in an organic solvent such as methanol able to solubilize curcumin in larger amounts. The diffusion coefficients of **3a** and **3b** obtained by DLS experiments are respectively $(1.18 \pm 0.02) \times 10^{-12}$ and

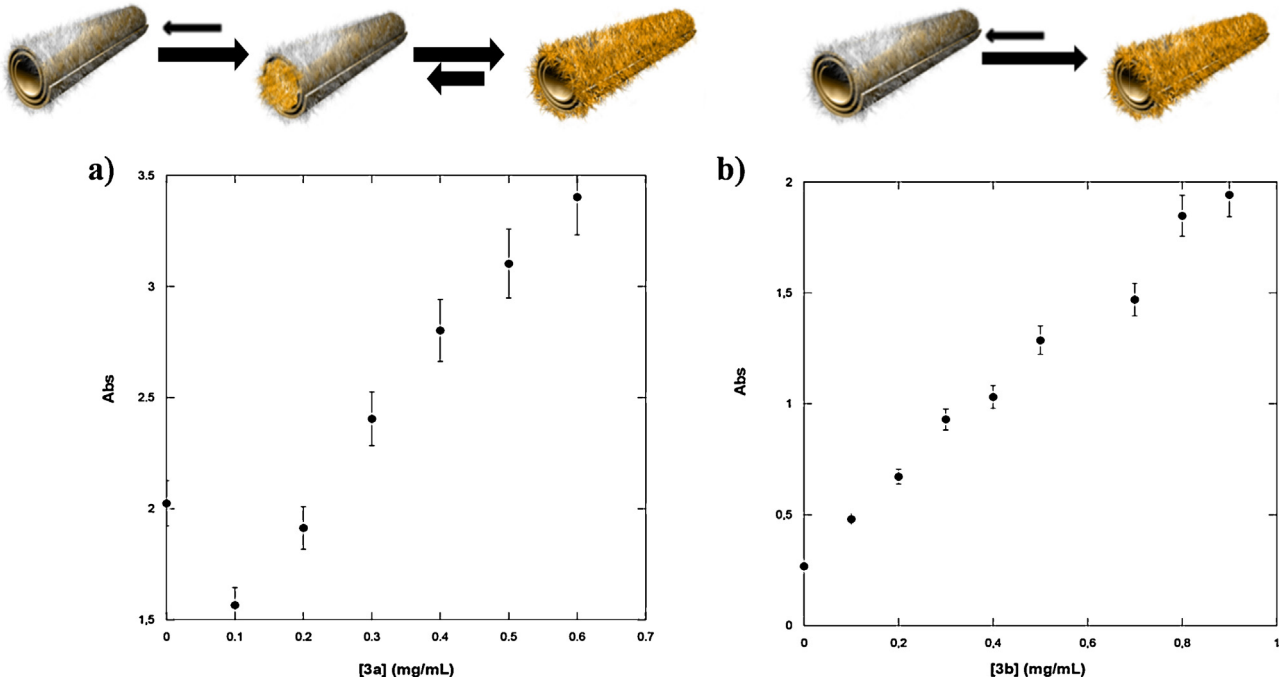

Fig. 3. Trend of the absorbance (λ_{max} = 440 nm) of the curcumin (1×10^{-4} M) as function of (a) **3a**, (b) **3b** concentration (from 0 to 1.8×10^{-3} g/mL) in H_2O/MeOH 9:1. The inset shows a representation cartoon of hypothesized equilibria.

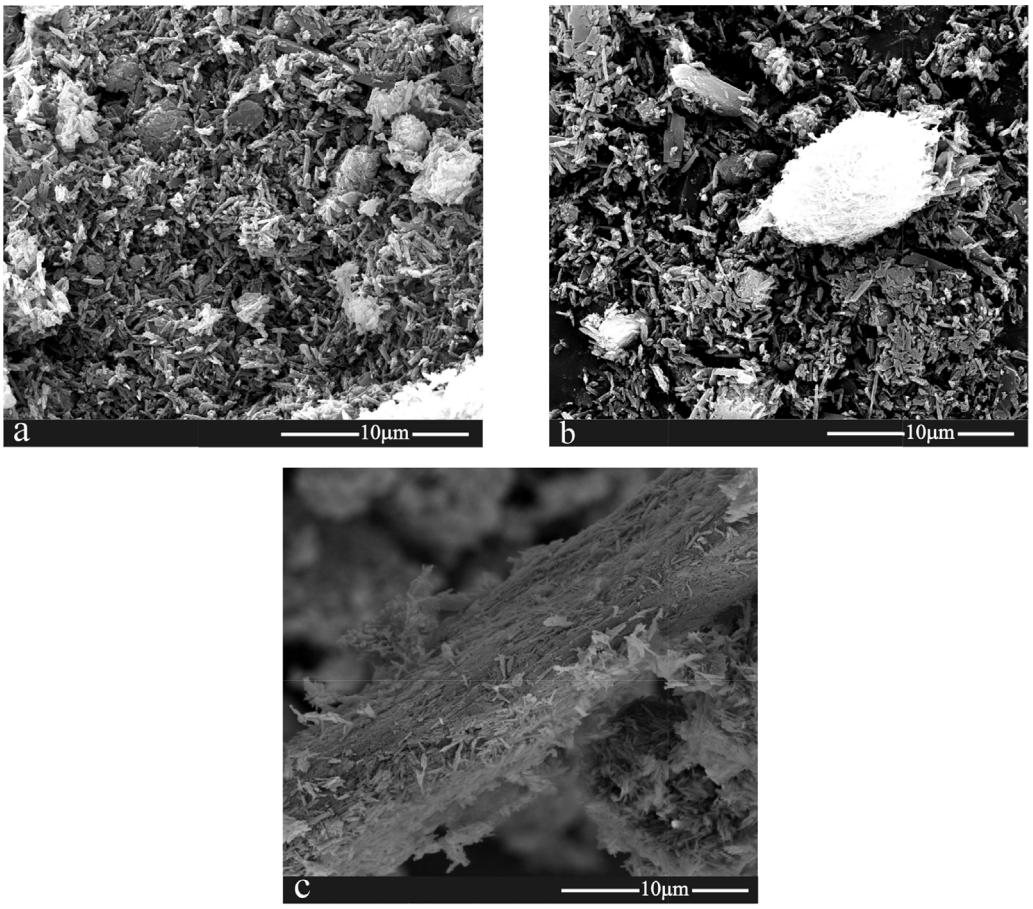

Fig. 4. SEM images for (a) **3a**/Curc; (b) **3b**/Curc; (c) p-HNT/Curc.

$(1.64 \pm 0.5) \times 10^{-13}\,m^2\,s^{-1}$ in water, and $(1.73 \pm 0.09) \times 10^{-12}$ and $(1.54 \pm 0.11) \times 10^{-12}\,m^2\,s^{-1}$ in methanol.

By comparing these results with the diffusion coefficient of p-HNT in water ($9.4 \times 10^{-13}\,m^2\,s^{-1}$) (Cavallaro et al., 2011) it appears that in methanol both **3a** and **3b** form no aggregates. This is not the case in water where the more hydrophobic substituent plays a role favoring the aggregation of nanotubes, as evidenced by the slower diffusion for **3b**. This result can be explained considering that water is a worse solvent for the most hydrophobic external modifier. The reduced diffusion dynamic was obtained for p-HNT by hydrophobic modification of the outer surface by means of a cationic surfactant (Cavallaro et al., 2012) and the nanotubes aggregation due to hydrophobic lateral interaction was claimed in that case. With the aim at evidencing possible changes in the nanoparticle–nanoparticle interactions, the ζ-potential in water was measured. Both samples **3a-b** showed close negative ζ-potential values (-19.5 ± 1.5 and -24.1 ± 0.9 mV, respectively) and therefore differences in the electrostatic nanoparticle–nanoparticle repulsions are probably negligible, confirming that the aggregation of compounds is driven by π–π and van der Waals interactions.

Based on our results, we planned to investigate the colloidal stability of **3b** in methanol/water mixed media. To this purpose diffusion coefficients were measured in a wide range of solvent compositions (Fig. 1). It is straightforward to note that **3b** is rather stable in the methanol rich regime, as it is proved by a value of the diffusion coefficient close to the one expected for monodispersed nanotubes. On the other hand, if the methanol concentration is lower than 8.4% (corresponding to 9:1 water/methanol volume ratio), diffusion is suddenly slowed down. In principle this effect can be due to: (i) change in the viscosity of the solvent medium;

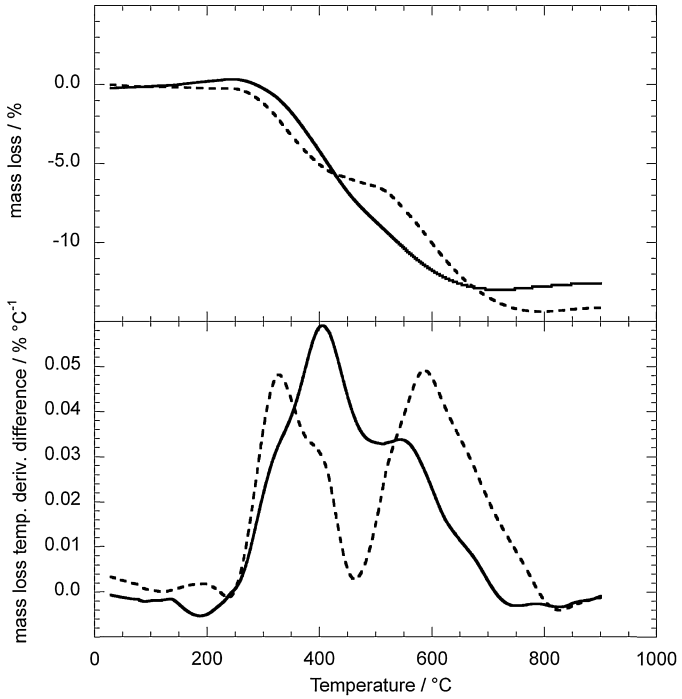

Fig. 5. Thermoanalytical curves of f-HNT**3a**/Curc (—) and f-HNT**3b**/Curc (—). The thermoanalytical curves were subtracted to f-HNT**3a-b** to show degradation peaks of curcumin.

(ii) the **3b** aggregation induced by π–π and van der Waals interactions between the external moieties.

To the light of the monotonic change of methanol/water mixture (Thompson et al., 2006), the aggregation occurs in our system.

3.3. Interactions between HNT and curcumin

The incorporation of curcumin in HNT formed a stable, strongly colored dispersion. Color indicates a homogeneous distribution of curcumin in the aqueous medium.

The interaction between p-HNT or **3a-b** compounds with curcumin was evaluated by DLS measurements and Uv–vis spectroscopy.

In order to highlight the interactions of **3a-b** with curcumin the diffusion dynamic of the modified nanotubes was studied as a function of the curcumin concentration in the mixed methanol/water solvent. The volume ratio water/methanol was fixed at 9:1 which is the best compromise between curcumin solubility and the stability of f-HNT dispersions (Fig. 1). The concentration dependence of the diffusion coefficient was negligible (see data in SI) and therefore average values of $(3.0 \pm 1.0) \times 10^{-13}\ m^2\ s^{-1}$ and $(6.0 \pm 3.0) \times 10^{-13}\ m^2\ s^{-1}$ were calculated for **3a** and **3b**, respectively. These results show a significant slowdown of both f-HNT nanoparticles in the presence of curcumin, indicating that the interaction favors the aggregation or networking of the nanotubes.

Considering the results obtained from DLS measurements, mentioned above, we recorded the UV–vis spectra of dispersion of p-HNT/curcumin (p-HNT/Curc) both in buffer pH 8 solution/methanol 9:1 mixture (λ_{max} = 360 nm) and a water/methanol 9:1 mixture (λ_{max} = 425 nm), at 25 °C and at a fixed concentration of curcumin (1×10^{-4} M) in the presence of increasing amounts of p-HNT (0–1.8×10^{-3} g/mL). The occurrence of the interaction was evaluated by measuring the absorbance at the maximum absorption wavelength of the curcumin in each mixed solvent. Typical trends are depicted in Fig. 2.

Two different behaviors were observed depending on the medium solvent used. In the buffer solution/methanol mixture (Fig. 2a) absorbances (recorded at 360 nm) decrease on increasing of p-HNT concentration. Moreover, after interaction with p-HNT, the p-HNT/Curc has a peak at the same absorption wavelength as free curcumin. These findings suggest that curcumin has been successfully encapsulated into the HNT lumen. Similar results are reported in literature for the encapsulation of curcumin within poly(amidoamine) dendrimers (Wang et al., 2013).

In the neutral H_2O/MeOH 9:1 mixture two absorbance maxima, at 260 and 425 nm were observed. The absorbance values at 425 nm decrease on increasing the amounts of p-HNT. By contrast, absorbances at 260 nm increase up to a p-HNT concentration of ca. 6×10^{-3} g/mL, and then reach a plateau at larger concentrations (Fig. 2b). These trends could indicate that two different equilibria occur in solution, i.e. the loading of curcumin into the lumen of p-HNT and its adsorption onto p-HNT external surface.

Similarly, we recorded the UV–vis spectra of f-HNT**3a-b**/Curc in mixed water/methanol 9:1 solvent, at 25 °C and a fixed concentration of curcumin (1×10^{-4} M) in the presence of varying amounts of compounds **3a-b** (0–9×10^{-4} g/mL). According to the previous observations, also in this case we remarked two different behaviors.

We observed an initial decrease of the absorbance value and then an increase on increasing the f-HNT concentration (Fig. 3a). As previously mentioned, we have hypothesized the coexistence of two different "curcumin species", one encapsulated and the other adsorbed onto external surface, of f-HNT. The initial decrease could be due to the encapsulation of curcumin in the **3a** lumen, whereas the subsequent increase in the absorbances may be attributed to the formation of an adsorbed complex. The introduction of a positive charge onto the external surface of f-HNT makes the curcumin being preferentially adsorbed onto the external surface, by means of more effective π–π and cation–π interactions. Unfortunately, in the latter case we could not obtain any data for the absorbance value at 260 nm because of the concomitant occurrence of the absorption band of the triazolium moieties present onto the f-HNT surface.

Fig. 3b shows the variation in the absorbance of curcumin as a function of **3b** concentration. In this case, we have supposed that the external functionalization, which has longer side alkyl chain length, contributes more to the adsorption of curcumin on the external surface.

3.3.1. Loading procedure

Loading HNT/Curc was made with two different procedures, depending on the p-HNT or f-HNT used. According to literature (Veerabadran et al., 2007) we performed a loading procedure from

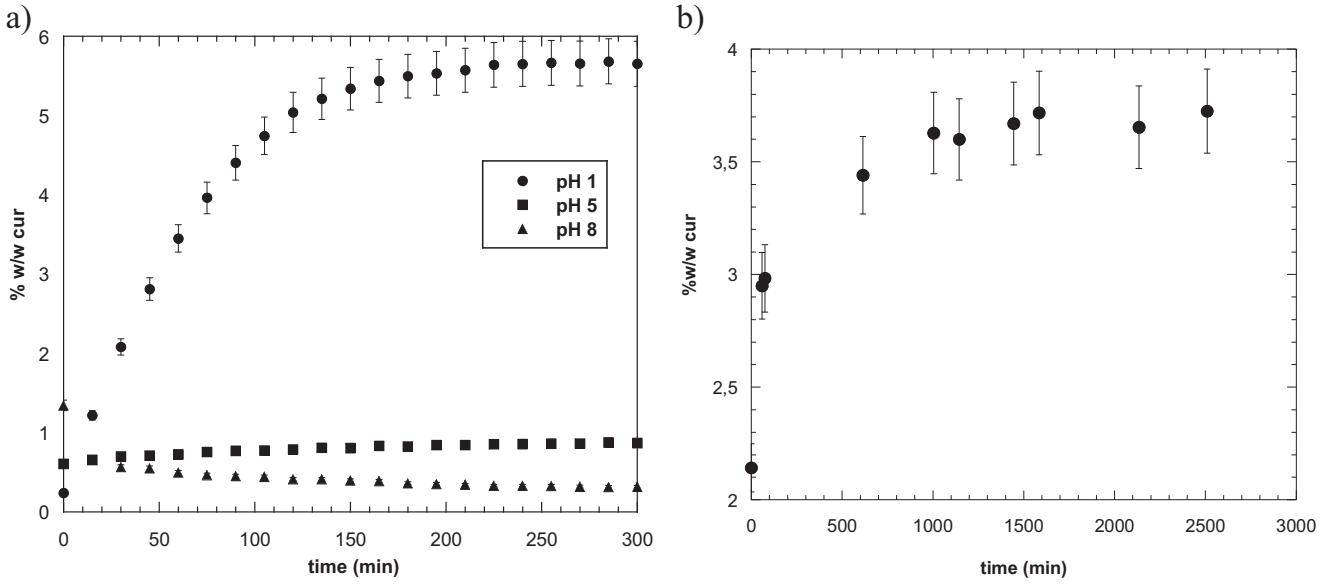

Fig. 6. Amount of curcumin released from (a) **3b** as a function of time for three different pH and (b) p-HNT/Curc system at pH 1.

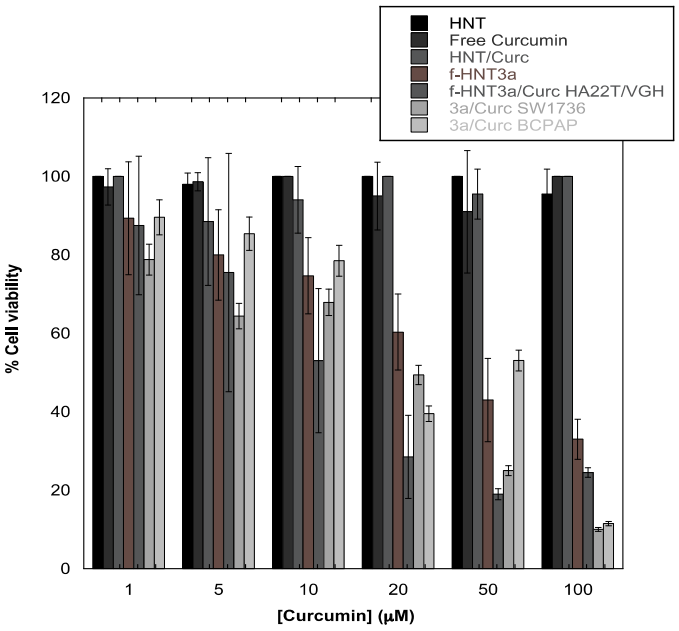

Fig. 7. MTS test for cell viability of HA22T/VGH, SW1736 and BCPAP cells cultured for 72 h in presence of free curcumin, **3a**, p-HNT/Curc and **3a**/Curc.

an aqueous solvent containing methanol, which provided higher solubility for the drug.

Loading of the p-HNT with curcumin was based on vacuum cycling of a halloysite suspension in a saturated solution containing curcumin, as described previously (Price et al., 2001; Abdullayev et al., 2009). This cycle was repeated several times in order to get the highest loading efficiency. After loading, the p-HNT/Curc complex was washed in order to remove any curcumin not interacting with p-HNT. Differently for f-HNT/Curc loading, the nanotubes (0.2 mg/mL) were left under constant stirring at room temperature in mixed water/methanol 9:1 solvent with curcumin at a concentration as larger as 10^{-5} M.

In both cases subsequent investigations were conducted on the dry solid filtered from dispersion, washed with water and dried overnight at 60 °C.

The obtained materials are imaged by SEM (Fig. 4) and it turned out that in the submicron range the typical tubular shape is preserved in all cases, whereas f-HNT and p-HNT loaded with curcumin showed a very different morphology in a larger length scale. In particular f-HNT/Curc did not show any peculiar organization while p-HNT/Curc presented a fiber-like structure. Each fiber was ca. 8 μm large in diameter and several millimeters long. Moreover, the presence of HNT within the fiber with the nanoparticles distributed without an apparent orientation is observed (Fig. 4c).

TGA experiments endowed to estimate the amount of curcumin in the solid materials.

This was determined by comparing the residual mass at 400 °C of each sample, and resulted to be as large as 1.5, 11.0 and 12.5% for p-HNT, **3a** and **3b** respectively. Besides the high loading obtained, it is very interesting to observe from TGA data that the degradation temperature of the organic moieties is dependent on the investigated system. In particular, the curcumin encapsulated in p-HNT shows a higher degradation temperature (536 °C) as compared to the pure compound (323 °C). This striking enhancement of the thermal stability can be due to encapsulation of the degradation products into the nanotube lumen (Cavallaro et al., 2011; Du et al., 2006). It is intriguing to notice that loaded f-HNT**3a-b** showed two differential degradation peaks for curcumin

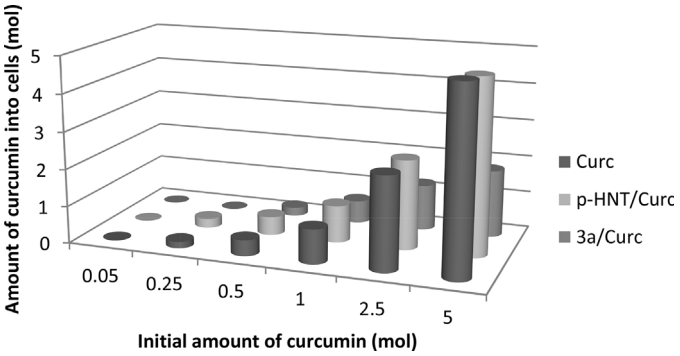

Fig. 8. Graphical representation of curcumin amount (mol) into the cells as a function of initial amount of curcumin (mol) for HA22T/VGH cell line.

(401 and 320 °C for **3a**; 570 and 320 °C for **3b**), which can be attributed to the molecules at the outer surface and incorporated into the cavity (Fig. 5). By comparing the data for loaded HNT and f-HNT one can assume that incorporated curcumin is present in the f-HNT and that the more hydrophobic modification generates a preferential interaction of the curcumin with the outer surface. The latter findings are in agreement with the UV–vis results.

3.4. Release kinetics

Controlled release is an attainable and desirable characteristic for a drug carrier. The factors affecting the drug release rate rely on the structure of the matrix where the drug is contained and the chemical properties associated with both the clay and the drug. The drug release is also diffusion controlled as the drug can travel through the pore of halloysite. The most desirable release profile would show a constant release rate with time (Vergaro et al., 2010).

pH is a key factor influencing the oral drug delivery. It is known that pH is about 1.2–2.0 in stomach, about 7.0 in small intestine and as high as 8 in the distal part (Shargel and Yu, 2012).

In Fig. 6 extended release profile of curcumin from f-HNT and p-HNT is elucidated.

The release of curcumin at pH 1 from compound **3b** reaches a plateau after 150 min, an initial burst is observed within 100 min followed by a prolonged release. The obtained result is outstanding because it is well known that curcumin suffers from chemical instability in the gastrointestinal tract.

Release profiles obtained at pH 5 and pH 8 showed in both cases only a small amount of curcumin released from the systems. The same conclusions can be drawn for compound **3a** (see SI).

As it can be seen there are significant difference for the release in different pH conditions, which can be explained as follows. A first factor to keep into account is the different solubility as a function of pH. Indeed curcumin molecules ($pK_{a1} = 8.38$, $pK_{a2} = 9.88$ and $pK_{a3} = 10.51$) can exist as cationic, neutral or anionic species in acidic, neutral or alkaline solution, respectively (Bernabé-Pineda et al., 2004). Therefore, curcumin can be easily migrated out of the carrier at pH 1 in its cationic form, resulting in a higher release as compared with that at pH 5.0 and 8.0.

The interaction of curcumin and f-HNT is another reason for the difference in drug release behavior. In acidic solution both f-HNT and curcumin are positively charged; therefore, electrostatic repulsions may also accelerate the release of drug from the f-HNT**3b**.

In the case of p-HNT (Fig. 6b), the release of curcumin at pH 1 showed a similar behavior than the release, at the same pH, from f-HNT.

Release of curcumin from HNT can be considered the phase of desorption of the previously adsorbed drug molecules from a

cylindrical matrix (Dash et al., 2010; Korsmeyer et al., 1983). In this solid/liquid interface process will be involved different simple interface processes leading to the transport of the drug from the solid to the liquid phase. These simple processes may be governed by diffusion and in our particular case are due to the desorption of the drug adsorbed on the external HNT surface.

To better understand the release mechanism of curcumin from the different carriers, we analyzed the experimental data obtained for f-HNT/**3b** with the following equations: first-order (2) and the Power law (3):

$$F_t = 1 - e^{-kt} \quad (2)$$

$$F_t = kt^n \quad (3)$$

where F_t is the drug release fraction at time t, k is the release constant of the respective equations, t is the release time and n is the characteristic diffusion exponent.

The correlation coefficient for Eq. (2), either for the release from p-HNT and f-HNT, is higher than the Power fit equation, so the release mode of curcumin, in both cases, follows the first-order kinetics.

3.5. Cells viability

In order to validate the efficiency of p-HNT/Curc and f-HNT **3a**/Curc on cell viability we tested a panel of 7 tumor cell lines, namely 8505C, BCPAP, C643, SW1736, HA22T/VGH, Hep3B and HepG2. We performed MTT and MTS tests in order to verify if the complexes are able to exert antitumoral action.

Cell viability was estimated at 24, 48 and 72 h under different curcumin concentrations (in the 1–100 μM range). It was observed that cell viability decreases in a concentration and time dependent way. The inhibition efficiency of the complex increased when the incubation time was prolonged from 24 to 72 h, the f-HNT **3a**/Curc displayed significantly stronger anticancer activity than free curcumin.

In Fig. 7 data regarding the antitumor effects of curcumin and its derivatives on the cell lines of hepatocarcinoma HA22T/VGH, anaplastic thyroid SW1736 and papillary thyroid BCPAP after 72 h of incubation are shown; the results obtained from treatment with f-HNT**3a** are reported for useful comparison.

The survival rates of the various tumor cells incubated with p-HNT at each concentration were found in the range of 96–100%, indicating they have no effect on cell viability of the tumor cell lines under the concentration conditions investigated. This result is not surprising because it is well known that HNT materials have no cytotoxic effects (Lai et al., 2013) whereas f-HNT**3a**, as it can be noticed from Fig. 7, exerts variable cytotoxic effects against the different cell lines with IC_{50} of 40.0 ± 14.6 μM. This different behavior could be due to the introduction of triazolium salts onto the carrier, that it is known to possess very interesting biological activities, in particular antitumoral effect (Pokhodylo et al., 2013).

It is known that nanoparticles enter cells through an internalization mechanism that presumably involves an endocytosis process, whereby f-HNT**3a** could be uptake into the cytosol by endosomes (Zhang et al., 2009).

Free curcumin has no effect on cell viability, probably due to its rapid metabolism and systemic elimination, which limits its clinical application (Anand et al., 2007).

No cytotoxic effects for the several cell lines in the presence of the complex p-HNT/Curc were observed. In our opinion the availability of curcumin encapsulated in the halloysite lumen is low, so it is not released in these conditions. Similar results were obtained by Leporatti et al. for resveratrol (Vergaro et al., 2010).

The f-HNT **3a**/Curc shows, at each concentration, a significantly higher cytotoxicity than free curcumin. In particular, the concentration of f-HNT**3a**/Curc which caused 50% inhibition of cell growth was 11.0 ± 6.4 μM for HA22T/VGH, 23.0 ± 8.6 μM for SW1736 and 23.1 ± 10.6 μM for BCPAP respectively. This increase in the cytotoxicity of f-HNT**3a**/Curc compared with free curcumin was probably due to the possibility of enhanced cellular uptake via endocytic process combined with enhanced aqueous solubility of f-HNT**3a**/Curc.

The increase in the cytotoxicity of f-HNT**3a**/Curc with respect to p-HNT/Curc can be explained as follows: (i) f-HNT**3a**/Curc has the largest curcumin loading; (ii) in the case of f-HNT**3a** is inside and outside the nanotubes, and therefore the drug can be released quickly from the carrier.

Fig. 8 shows the amount of curcumin that is embedded in the HA22T/VGH cells after treatment with free curcumin, p-HNT/Curc and f-HNT**3a**/Curc.

Despite free curcumin enters almost totally in the cells, it has no effect on cell viability probably because it is rapidly degraded as a consequence of its instability in the culture medium (Wang et al., 2008).

On the contrary, when cells were treated with **3a**/Curc, we observe that curcumin enters in the cells until the concentration reaches the IC_{50} value. This may indicate that it is necessary a low amount of drug to exert a therapeutic activity.

Based on the cytotoxicity assays, we summarized the IC_{50} values for f-HNT**3a**/Curc against each cell lines after an incubation time of 72 h. It was found that the complex is active against several tumor cell lines (data are shown in Table S.1 in Supporting information).

It is noteworthy that f-HNT **3a**/Curc is extremely effective toward both differentiated and undifferentiated tumor cell lines. This observation results particularly important on considering that at present there is no antitumoral chemiotherapic drug against anaplastic thyroid cancer (ATC) and survival of patients is less than 1 year. Moreover for resistant cell lines, such as the hepatic cancer HA22T/VGH cell, curcumin was usually administered in combination with other chemiotherapic agents to achieve synergistic antitumor effect (Notarbartolo et al., 2005; Ganta and Amiji, 2009).

4. Conclusions

We have successful modified the external surface of halloysite with triazolium salts.

The new materials obtained were characterized by means of FTIR spectroscopy, TGA, SEM and ζ-potential measurements that confirm the presence of triazolium moiety. With the aim to employ them as carrier for curcumin, we tested their aqueous stability by turbidimetric analysis and DLS measurements. The interaction with the potential drug was evaluated by DLS and UV–vis spectroscopy. The results obtained confirmed the coexistence of different “curcumin species” depending on the system considered; one encapsulated and one adsorbed onto halloysite. Release kinetics showed that the new systems have a different release profiles depending on pH of the medium.

These systems have the advantage of high drug encapsulation efficiency, as well as controlled and sustained release capabilities; moreover, the triazole moiety, into the HNT surface, was found to have a synergic effect with curcumin, which make f-HNT an ideal carrier for anti-cancer therapies as confirmed by MTT and MTS assays.

Assays performed on a large panel of cancer cell lines to valuate cytotoxic effects of curcumin and its derivatives, showed that the complex f-HNT **3a**/Curc is active in several tumor models.

Additional material

Additional material IR spectra, TGA, DLS and turbidimetric data, kinetic release and IC_{50}.

Author contributions

The manuscript was written through contributions of all authors. All authors have given approval to the final version of the manuscript.

Competing interest

The authors declare that they have no competing interests.

Acknowledgment

The work was financially supported by the University of Palermo and PRIN 2010–2011 (prot. 2010329WPF).

Appendix A. Supplementary data

Supplementary data associated with this article can be found, in the online version, at http://dx.doi.org/10.1016/j.ijpharm.2014.09.019.

References

Abdullayev, E., Price, R.R., Shchukin, D., Lvov, Y.M., 2009. Halloysite tubes as nanocontainers for anticorrosion coating with benzotriazole. Appl. Mater. Interfaces 1, 1437–1443.
Aggarwal, S., Ichikawa, H., Takada, Y., Sandur, S.K., Shishodia, S., Aggarwal, B.B., 2008. Curcumin downregulates expression of cell proliferation: antiapoptotic and metastatic gene products through suppression of IκBa kinase and AKT activation. Mol. Pharmacol. 69, 195–206.
Al-Masoudi, I.A., Al-Soud, Y.A., Al-Salihi, N.J., Al-Masoudi, N.A., 2006. 1,2,4-Triazoles: synthetic approaches and pharmacological importance. Chem. Heterocycl. Compd. 42, 1377–1403.
Anand, P., Kunnumakkara, A.B., Newman, R.A., Aggarwal, B.B., 2007. Bioavailability of curcumin: problems and promises. Mol. Pharm. 4, 807–818.
Bagihalli, G.B., Avaji, P.G., Patil, S.A., Badami, P.S., 2008. Eur. J. Med. Chem. 43, 2639–2649.
Bates, T.F., Hildebrand, F.A., Swineford, A., 1950. Morphology and structure of endellite and halloysite. Am. Mineral. 35, 463–484.
Bernabé-Pineda, M., Ramìrez-Silva, M.T., Romero-Romo, M., Gonzàlez-Vergara, E., Rojas-Hernàndez, A., 2004. Determination of acidity constants of curcumin in aqueous solution and apparent rate constant of its decomposition. Spectrochim. Acta A: Mol. Biomol. Spectrosc. 60, 1091–1097.
Cavallaro, G., Lazzara, G., Milioto, S., 2011. Dispersions of nanoclays of different shapes into aqueous and solid biopolymeric matrices: extended physicochemical study. Langmuir 27, 1158–1167.
Cavallaro, G., Lazzara, G., Milioto, S., 2012. Exploitong the colloidal stability and solubilization ability of clay nanotubes/ionic surfactant hybrid nanomaterials. J. Phys. Chem. C 116, 21932–21938.
Chen, H.-W., Lee, J.-Y., Huang, J.-Y., Wang, C.-C., Chen, W.-J., Su, S.-F., Huang, C.-W., Ho, C.-C., Chen, J.J.W., Tsai, M.-F., Yu, S.-L., Yang, P.-C., 2008. Curcumin inhibits lung cancer cell invasion and metastasis through the tumor suppressor HLJ1. Cancer Res. 68, 7428–7438.
Choi, H., Chun, Y.S., Kim, S.W., Kim, M.S., Park, J.W., 2006. Curcumin inhibits hypoxia-inducible factor-1 by degrading aryl hydrocarbon receptor nuclear translocator: a mechanism of tumor growth inhibition. Mol. Pharmacol. 70, 1664–1671.
Dash, S., Murthy, P.N., Nath, L., Chowdury, P., 2010. Kinetic modelling on drug release from controlled drug delivery systems. Acta Pol. Pharm.-Drug Res. 67, 217–223.
Du, M., Guo, B., Jia, D., 2010. Newly emerging applications of halloysite nanotubes: a review. Polym. Int. 59, 574–582.
Du, M., Guo, B., Jia, D., 2006. Thermal stability and flame retardant effects of halloysite nanotubes on poly(propylene). Eur. Polym. J. 42, 1362–1369.
Duan, J., Zhang, Y., Han, S., Chen, Y., Li, B., Liao, A., Chen, W., Deng, X., Zhao, J., Huang, B., 2010. Synthesis and in vitro/in vivo anti-cancer evaluation of curcumin-loaded chitosan/poly(butyl cyanoacrylate) nanoparticles. Int. J. Pharm. 400, 211–220.
Feng, S.S., 2004. Nanoparticles of biodegradable polymers for new-concept chemotherapy. Expert Rev. Med. Devices 1, 115–125.
Finn, M.G., Fokin, V.V., 2010. Click chemistry: function follows form. Chem. Soc. Rev. 39, 1231–1232.
Ganta, S., Amiji, M., 2009. Co-administration of paclitaxel and curcumin in nanoemulsion formulations to overcome multidrug resistance in tumor cells. Mol. Pharm. 6, 928–939.
Guo-Qiang, H., Li-Li, H., Song-Qiang, X., Wen-Long, H., 2008. Design: synthesis and antitumor activity of asymmetric bis(s-triazole Schiff-base)s bearing functionalized side-chain. Chin. J. Chem. 26, 1145–1149.
Horiuchi, S., Hanada, T., Ebisawa, M., Matsuda, Y., Kobayashi, M., Takahara, A., 2009. Contamination-free transmission electron microscopy for high-resolution carbon elemental mapping of polymers. ACS Nano 3, 1297–1304.
Huisgen, R., 1963. 1,3-Dipolar cycloadditions. Past and future. Angew. Chem. Int. Ed. Engl. 2, 565–598.
Jin, J.Y., Zhang, L.X., Zhang, A.J., Lei, X.X., Zhu, J.H., 2007. Synthesis and biological activity of some novel derivatives of 4-amino-3-(D-galactopentitol-1-yl)-5-mercapto-1,2,4-triazole. Molecules 12, 1596–1605.
Karl, A., Buder, W., 1983. US Patent 4401598.
Kim, T.H., Jiang, H.H., Youn, Y.S., Park, C.W., Tak, K.K., Lee, S., Kim, H., Jon, S., Chen, X., Lee, K.C., 2011. Preparation and characterization of water soluble albumin-bound curcumin nanoparticles. Int. J. Pharm. 403, 285–291.
Korsmeyer, R.W., Gurny, R., Doelker, E., Buri, P., Peppas, N.A., 1983. Mechanisms of solute release from porous hydrophilic polymers. Int. J. Pharm. 15, 25–35.
Kurien, B.T., Singh, A., Matsumoto, H., Scofield, R.H., 2007. Improving the solubility and pharmacological efficacy of curcumin by heat treatment. Assay Drug Dev. Technol. 5, 567–576.
Lai, X., Agarwal, M., Lvov, Y.M., Pachpande, C., Varahramyan, K., Witzmann, F.A., 2013. Proteomic profiling of halloysite clay nanotube exposure in intestinal cell co-culture. J. Appl. Toxicol. 33, 1316–1329.
Li, C., Liu, J., Qu, X., Guo, B., Yang, Z., 2008. Polymer-modified halloysite composite nanotubes. J. Appl. Polym. Sci. 110, 3638–3643.
Lin, Y.G., Kunnumakkara, A.B., Nair, A., Merritt, W.M., Han, L.Y., Armaiz-Pena, G.N., Kamat, A.A., Spannuth, W.A., Gershenson, D.M., Lutgendorf, S.K., Aggarwal, B.B., Sood, A.K., 2007. Curcumin inhibits tumor growth and angiogenesis in ovarian carcinoma by targeting the nuclear factor-κB pathway. Clin. Cancer Res. 13, 3423–3430.
Lvov, Y., Price, R.R., Gaber, B., Ichinose, I., 2002. Thin film nanofabrication via layer-by-layer adsorption of tubule halloysite spherical silica, proteins and polycations. Colloid Surf. A-Physicochem. Eng. Asp. 198, 375–382.
Matsuno, R., Otsuka, H., Takahara, A., 2006. Polystyrene-grafted titanium oxide nanoparticles prepared through surface-initiated nitroxide-mediated radical polymerization and their application to polymer hybrid thin films. Soft Matter 2, 415–421.
Ma, W., Otsuka, H., Takahara, A., 2011. Poly(methyl methacrylate) grafted imogolite nanotubes prepared through surface-initiated ARGET ATRP. Chem. Commun. 47, 5813–5815.
Ma, W., Yah, W.O., Otsuka, H., Takahara, A., 2012. Application of imogolite clay nanotubes in organic–inorganic nanohybrid materials. J. Mater. Chem. 22, 11887–11892.
Madejova, J., Komadel, P., 2001. Baseline studies of the clay mineral society source clays: infrared methods. Clay Clay Miner. 49, 410–432.
Massaro, M., Riela, S., Cavallaro, G., Gruttadauria, M., Milioto, S., Noto, R., Lazzara, G., 2014a. Eco-friendly functionalization of natural halloysite clay nanotube with ionic liquids by microwave irradiation for Suzuki coupling reaction. J. Organomet. Chem. 749, 410–417.
Massaro, M., Riela, S., Lazzara, G., Gruttadauria, M., Milioto, S., Noto, R., 2014b. Green conditions for the Suzuki reaction using microwave irradiation and a new HNT supported ionic liquid-like phase (HNT-SILLP) catalyst. Appl. Organomet. Chem. 28, 234–238.
Matsuno, R., Yamamoto, K., Otsuka, H., Takahara, A., 2003. Polystirene-grafted magnetite nanoparticles prepared through surface-initiated nitroxyl-mediated radical polymerization. Chem. Mater. 15, 3–5.
Meldal, M., Tornoe, C.W., 2008. Cu-catalyzed azide-alkyne cycloaddition. Chem. Rev. 108, 2952.
Noël, R., Song, X., Jiang, R., Chalmers, M.J., Griffin, P.R., Kamenecka, T.M., 2009. Efficient methodology for the synthesis of 3-amino-1,2,4-triazoles. J. Org. Chem. 74, 7595–7597.
Notarbartolo, M., Poma, P., Perri, D., Dusonchet, L., Cervello, M., D'Alessandro, N., 2005. Antitumor effects of curcumin alone or in combination with cisplatin or doxorubicin, on human hepatic cancer cells. Analysis of their possible relationship to changes in NF-kB activation levels and in IAP gene expression. Cancer Lett. 224, 53–65.
Pokhodylo, N., Shyyka, O., Matiychuck, V., 2013. Synthesis of 1,2,3-triazole derivatives and evaluation of their anticancer activity. Sci. Pharm. 81, 663–676.
Price, R.R., Gaber, B.B., Lvov, Y.M., 2001. In-vitro release characteristics of tetracycline HCl, khellin and nicotinamide adenine dineculeotide from halloysite: a cylindrical mineral. J. Microencapsul. 18, 713–722.
Rezaei, Z., Khabnadideh, S., Pakshir, K., Hossaini, Z., Amiri, F., Assadpour, E., 2009. Design synthesis, and antifungal activity of triazole and benzotriazole derivatives. Eur. J. Med. Chem. 44, 3064–3067.
Shargel, L., Yu, A., 2012. Applied Biopharmaceutics and Pharmacokinetics. McGraw Hill, New York.
Shenoy, D.B., Amiji, M.M., 2005. Poly(ethylene oxide)-modified poly(varepsilon-caprolactone) nanoparticles for targeted delivery of tamoxifen in breast cancer. Int. J. Pharm. 293, 261–270.
Singh, K., Singh, D.P., Barwa, M.S., Tyagi, P., Mirza, Y., 2006. Antibacterial Co(II), Ni(II), Cu(II) and Zn(II) complexes of Schiff bases derived from fluorobenzaldehyde and triazoles. J. Enzyme Inhib. Med. Chem. 21, 557–562.

Tang, H., Murphy, C.J., Zhang, B., Shen, Y., Sui, M., Van Kirk, E.A., Feng, X., Murdoch, W.J., 2010. Amphiphilic curcumin conjugate-forming nanoparticles as anticancer prodrug and drug carriers: in vitro and in vivo effects. Nanomedicine 5, 855–865.

Terayama, Y., Kikuchi, M., Kobayashi, M., Takahara, A., 2010. Well-defined poly (sulfobetaine) brushes prepared by surface-initiated ATRP using a fluoroalcohol and ionic liquids as the solvents. Macromolecules 44, 104–111.

Thompson, J.W., Kaiser, J.W., Jorgenson, J.W., 2006. Viscosity measurements of methanol-water and acetonitrile-water mixtures at pressures up to 3500 using a novel capillary time-of-flight viscometer. J. Chromatogr. A 1134, 201–209.

Tonle, I.K., Ngameni, E., Njopwouo, D., Carteret, C., Walcarius, A., 2003. Functionalization of natural smectite-type clays by grafting with organosilane: physico-chemical characterization and application to mercury(II) uptake. Phys. Chem. Chem. Phys. 5, 4951–4961.

Vansant, E.F., Van Der Voort, P., Vrancken, K.C., 1995. Characterization and Chemical Modification of the Silica Surface, 93. Elsevier, New York.

Veerabadran, N.G., Price, R.R., Lvov, Y.M., 2007. Clay nanotubes for encapsulation and sustained release of drugs. Nano 2, 115–120.

Vergaro, V., Abdullayev, E., Lvov, Y.M., Zeitoun, A., Cingolani, R., Rinaldi, R., Leporatti, S., 2010. Cytocompatibility and uptake of halloysite clay nanotubes. Biomacromolecules 11, 820–826.

Wang, L.-P., Wang, Y.-P., Pei, X.-W., Peng, B., 2008. Synthesis of poly(methyl methacrylate)-b-poly(*N*-isopropylacrylamide) (PMMA-b-PNIPAM) amphiphilic diblock copolymer brushes on halloysite substrate via reverse ATRP. React. Funct. Polym. 68, 649–655.

Wang, L., Xu, X., Zhang, Y., Zhang, Y., Zhu, Y., Shi, J., Sun, Y., Huang, Q., 2013. Encapsulation of curcumin within poly(amidoamine) dendrimers for delivery to cancer cells. J. Mater. Sci. Mater. Med. 24, 2137–2144.

White, L.D., Tripp, C.P., 2000. An infrared study of the amine-catalyzed reaction of methoxymethylsilanes with silica. J. Colloid Interface Sci. 227, 237–243.

Yuan, P., Southon, P.D., Liu, Z., Green, M.E.R., Hook, J.M., Antill, S.J., Kepert, C.J., 2008. Functionalization of halloysite clay nanotubes by grafting with γ-aminopropyltriethoxysilane. J. Phys. Chem. C 112, 15742–15751.

Zhang, S., Li, J., Lykotrafitis, G., Bao, G., Suresh, S., 2009. Size-dependent endocytosis of nanoparticles. Adv. Mater. 21, 419–424.